Energy Reports 11 (2024) 3436–3449

Contents lists available at ScienceDirect

Energy Reports

journal homepage: www.elsevier.com/locate/egyr

Research paper

Distributionally robust PV planning and curtailment considering cyber attacks on electric vehicle charging under PV/load uncertainties

Panggah Prabawa, Dae-Hyun Choi *

School of Electrical and Electronics Engineering, Chung-ang University, Dongjak-gu, Seoul 156-756, Republic of Korea

ARTICLE INFO

Keywords:
Distributionally robust optimization
Electric vehicle charging station
Uncertainty
Load altering attack
Volt/VAR optimization

ABSTRACT

A manipulated charging behavior of electric vehicles (EVs) due to an adversary along with the uncertain photovoltaic (PV) generation outputs and loads may lead to unstable power distribution system operations with voltage and current violations. To resolve this issue, this paper proposes an optimization framework where the following two types of uncertainties are addressed: (i) the natural uncertainties of PV generation outputs/loads and (ii) artificial uncertainties of load altering attacks (LAAs) on EV charging stations (EVCSs) via the manipulation of EV charging control signals. The proposed framework is formulated as a Wasserstein metric-integrated distributionally robust optimization (DRO)-based Volt/VAR optimization (VVO) problem. The proposed DRO-based VVO framework combined with PV planning and curtailment aims to minimize substation energy and voltage imbalance along with the complete removal of the constraint violations while handling uncertain PV generation outputs/loads and LAAs. To use off-the-shelf optimization solvers, tractable reformulation of the chance constraints of the voltage, current, and curtailed PV real power of the original DRO problem is provided. Numerical examples tested over IEEE 13-bus and 37-bus systems with PV systems and EVCSs show the efficiency of the proposed DRO framework in terms of substation energy, voltage imbalance, and PV planning/curtailment cost under stochastic LAAs.

1. Introduction

Recently, distributed energy resources such as solar photovoltaic (PV) systems and electric vehicles (EVs) at EV charging stations (EVCSs) have been increasingly deployed to ensure stable and economical power distribution system operations. To this end, distribution system operators (DSOs) perform Volt/VAR optimization (VVO) as a key step in distribution management (Singh et al., 2020). From the perspective of distribution grid operation, VVO aims to minimize power losses and voltage violations by exploiting the reactive power capability of PV systems via their smart inverters under various loads including charging of EVs (Nguyen and Choi, 2023). In addition, from the perspective of distribution grid planning, PV planning, which includes the optimal placement/capacity sizing of PV systems (Cai et al., 2020) and PV real power curtailment (Schermeyer et al., 2018) is essential for ensuring reliable grid operations and avoiding economic losses when a large number of PV systems are penetrated.

Notably, the following two factors may threaten efficient distribution grid operation and planning based on PV systems: (i) natural uncertainties in PV generation outputs and loads and (ii) artificial uncertainties of malicious cyber-attacks on distribution grids. With the growing penetration of PV systems and various controllable loads such as EVs in a distribution grid, the stability of distribution grid operations can be increasingly threatened owing to inadequate handling of their inherent uncertainties (e.g., intermittent PV generation outputs and random arrival/departure times of EVs). Furthermore, the increasingly realistic cyber-attacks on distribution grids may result in large-scale blackouts and severe economic losses. For example, the cyber-attacks in Ukraine in 2015, based on the manipulation of the control signals of generators and circuit breakers transmitted by DSOs, led to an extensive blackout (Liang et al., 2017). To address such issues, this study aims to develop a natural and artificial uncertainty-aware optimization framework, in which the impact of cyber-attacks on EVCSs through the manipulation of EV charging control signals is mitigated by PV planning and curtailment under uncertain PV generation outputs and loads. The research relevant to this study can be summarized in the following three categories.

- *PV planning and curtailment:* Researchers formulated an optimization problem for determining the optimal location and size of distributed generators (DGs) including PV systems (Al Abri et al., 2013), in which the voltage stability margin is improved while considering probabilistic DG generation and load characteristics.

* Corresponding author.
E-mail address: dhchoi@cau.ac.kr (D.-H. Choi).

https://doi.org/10.1016/j.egyr.2024.03.025
Received 13 October 2023; Received in revised form 4 January 2024; Accepted 9 March 2024
Available online 12 March 2024

Nomenclature

The main notations used throughout this paper are summarized here. Bold symbols represent vectors or matrices. Other undefined symbols are explained in the text.

Sets and indices

$\mathcal{N}$	Set of buses in a distribution system.
$\mathcal{N}^{\text{EVCS}}$	Set of buses with EVCSs.
$\mathcal{N}^{\text{L}}$	Set of buses with loads.
$\mathcal{N}^{\text{PV}}$	Set of buses with PV systems.
$\mathcal{T}$	Set of scheduling time horizon.
$\boldsymbol{\Phi}$	Set of phases.
ϕ	Index of phase where $\phi \in \boldsymbol{\Phi}$.
E	Index of EVCS where $E \in \mathcal{N}^{\text{EVCS}}$.
e	Index of EV at EVCS E where $e \in \mathcal{N}_E^{\text{EVCS}}$.
i	Index of bus where $i \in \mathcal{N}$.
ij	Index of line from bus i to j where $i, j \in \mathcal{N}$.
l	Index of load where $l \in \mathcal{N}^{\text{L}}$.
p	Index of PV system where $p \in \mathcal{N}^{\text{PV}}$.
t	Index of scheduling time where $t \in \mathcal{T}$.

Parameters

$\mathbf{a}, \mathbf{b}, \mathbf{c}, \mathbf{d}_{ij}$	Parameter vectors for the linear power flow model.
$\mathbf{E}_{ij}, \mathbf{B}_{ij}$	Auxiliary matrices.
$\mathbf{M}, \mathbf{K}, \mathbf{G}, \mathbf{J}_{ij}$	Parameter matrices for the linear power flow model.
$\mathbf{w}, \mathbf{W}$	Three-phase zero-load vector and matrix.
$\mathbf{Y}$	Three-phase bus admittance matrix.
π_1	Price of PV system installation.
π_2	Price of PV system capacity upgrade.
π_3	Price of PV generation output curtailment.
ψ	Coefficient of PV reactive power limit.
$\widehat{p}(\widehat{q})^{\text{load}}$	Predicted real(reactive) power demand.
$\widehat{p}^{\text{EVCS}}$	Predicted EVCS real power demand.
$\widehat{p}^{\text{EV}}$	Sampled EV charging demand.
$\widehat{p}^{\text{PV}}$	Predicted PV real power generation output.
$\widehat{x}^{\text{EV}}$	Predicted binary EV charging signal.
$\widehat{z}$	Binary location status for existing PV system.
$i_{ij}^{\text{min(max)}}$	Minimum(maximum) current magnitude at line ij.
$p^{\text{PV,max}}$	Maximum PV real power output.
$s^{\text{PV,+,max}}$	Maximum additional PV capacity.
$u(\gamma)^{\text{PV}}$	Coefficient of PV capacity(curtailment).
$v^{\text{min(max)}}$	Minimum(maximum) voltage magnitude.

Variables

$\mathbf{i}_{ij,t}$	Vector of complex current at line ij and time t.
$\mathbf{s}_{s,t}$	Vector of complex power at substation s and time t.
$\mathbf{v}_t$	Vector of complex voltages at time t.
i	Complex current.
$p(q)^{\text{inj}}$	Real(reactive) power injection.
$p^{\text{PV,c}}$	Curtailed PV real power.
$q(s)^{\text{PV}}$	PV reactive(apparent) power output.
$s^{\text{PV,+}}$	Added PV capacity.
z	Binary location status for added PV system.

A probability-weighted robust optimization method was developed (Zhang et al., 2018b), in which the total profit of the DSO is maximized by optimally allocating DGs in microgrids along with the modeling of uncertainties in the DG generation and load.

Furthermore, a two-stage stochastic programming optimization problem was formulated (Zhang et al., 2018a), in which the optimal locations and sizes of the PV systems and EVCSs are determined in a coupled transportation and power network. The solving time of the optimization problem was reduced using a generalized Benders decomposition algorithm. Moreover, a probabilistic approach for maximizing the hosting capacity of PV systems was proposed (Ali et al., 2021), in which the size of the PV system inverter for the watt-VAR function is optimized with the incorporated inverter reactive power capability. Other researchers proposed an optimal charging and discharging strategy (Kim et al., 2020) using energy storage systems to minimize PV power curtailment and maximize the profit of PV power producers. In Liu et al. (2020), several household-centric indices were introduced to fairly evaluate the influence of various PV curtailment schemes on residential distribution networks in terms of PV harvesting, energy export, and financial benefits. An approach to plan the PV sizing and utilize the PV curtailment using steady-state security region was proposed (Sun et al., 2022) to economically improve the penetration of renewable energies into the distribution system. In Wang et al. (2024), a joint planning method of PV installation size and location with wind turbine and multi-timescale flexible resources was proposed for economical investments and operating costs.

- *Cyber-attacks on EVCSs:* To exploit the vulnerability of internet-based smart grid applications, load altering attacks (LAAs) (Mohsenian-Rad and Leon-Garcia, 2011) have been devised to compromise the control signals for the optimal operation of controllable loads including EVs. Compared with the cyber-attacks on power grids based on communication networks and control centers, such as switching attacks (Liang et al., 2019), denial-of-service attacks (Cheng et al., 2022), false data injection attacks on state estimation (Tran et al., 2021), and direct control signal manipulation on EVCS (Basnet and Ali, 2023), LAAs are more realistic because they manipulate only the control signal without breaking through communication network and control center. In LAA-based EVCS attack (ElHussini et al., 2021), a sudden surge in the power demand and supply of EVCSs occurs through the LAA-based switching manipulation of EV charging and discharging. Researchers (Acharya et al., 2020b) also developed a novel LAA that injects a botnet malware into EVs and EVCSs, resulting in undervoltage and power outages in the distribution grid. In an LAA-based optimization framework (Acharya et al., 2020a), the adversary compromises the EV charging commands and suddenly decreases the demand in the power grid, resulting in an over-frequency grid condition. Furthermore, a two-stage optimization problem was formulated for mitigating the adverse impact of LAAs on the distribution grid via EV charging signal distortion (Liu and Wang, 2022). The researchers determined the optimal location/size and operation status of soft open point devices to maintain a normal voltage profile in the event of LAAs.
- *Uncertainty-aware optimization for power system operation:* Conventionally, stochastic optimization (SO) (Kou et al., 2018; Budiman et al., 2022) and robust optimization (RO) techniques (Jabr, 2013) have been adopted to address the uncertainties in power system operations. However, SO requires prior knowledge of the

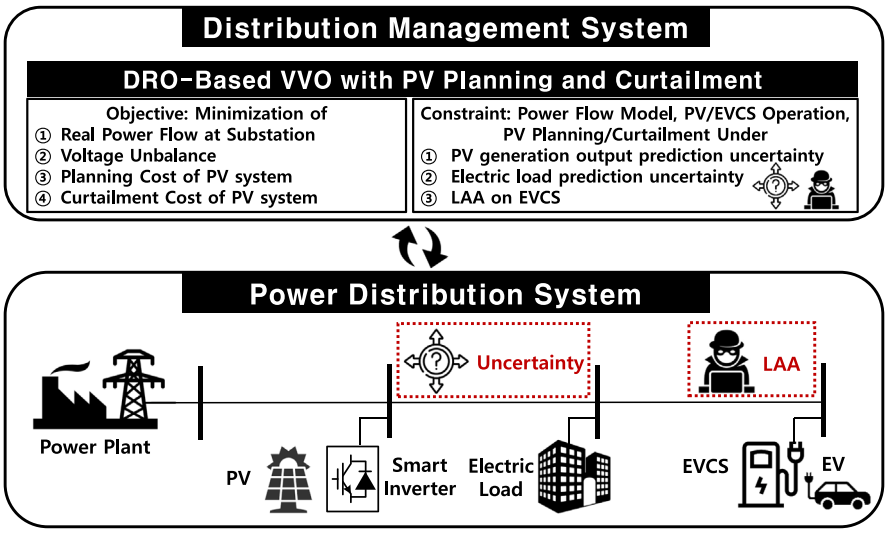

Fig. 1. Model of the proposed framework for DRO-based VVO with PV planning and curtailment.

true distribution of uncertain parameters, and RO yields an excessively conservative solution based on the worst-case situation. To address these limitations, distributionally robust optimization (DRO) has emerged (Gao and Kleywegt, 2023). Because DRO uses the Wasserstein metric, knowledge of the true distribution of uncertain parameters is not required, and a less conservative robust solution is obtained using an ambiguity set consisting of the potential distributions of uncertain parameters (Xie, 2019). Thus, the Wasserstein-based DRO method has the following advantages: (i) tractable reformulation, (ii) asymptotic consistency, and (iii) finite sample guarantee. The DRO method has been used to realize power flow optimization (Guo et al., 2019), multi-energy system operation in wholesale electricity markets (Nasiri et al., 2023), microgrid operation integrated with hydrogen fueling station (Wu et al., 2019), prosumer energy management (Guo et al., 2022), and conservation voltage reduction using the data enriched method that recovers the high-resolution PV generation and load data (Zhang et al., 2024).

However, the previous studies on mitigating the impact of LAAs on power distribution systems have the following limitations. First, most of the LAA-mitigation methods were formulated in a deterministic optimization (DO) problem that does not explicitly take into account uncertainty. Since the natural uncertainties associated with PV generation output and load demand exist in real-world power distribution systems, the DO method may not calculate accurate mitigation solution of LAAs on such realistic power system operation. Second, the existing works exploited PV planning and curtailment to ensure stable and profitable power distribution system operations in the presence of no LAAs; however, the PV flexibility can be potentially utilized to maintain robust distribution system planning/operation against LAAs through PV planning and curtailment. Third, the existing frameworks can be applied only to balanced distribution systems; however, actual distribution systems are inherently unbalanced.

To overcome these limitations, this paper proposes a DRO framework in which the DSO performs a PV planning/curtailment-integrated VVO in a realistic three-phase unbalance distribution system while handling both the uncertain PV generation output/load and LAA on EVCS. A key part of the proposed DRO framework is to incorporate PV planning and curtailment process into VVO to ensure reliable and robust distribution grid planning and operation against the PV generation output/load and LAA uncertainties. For PV system, the planning and operation are simultaneously realized as follows. In the planning stage, the optimal PV deployment factors, such as the optimal size and location, are determined. Subsequently, the real power generated by the PV panels is optimally curtailed to satisfy operational constraints within a short-term interval (e.g., every 5 min) followed by a typical VVO. The key contributions of this study can be summarized as follows:

- *Development of a DRO-based VVO model under uncertainties:* In contrast with conventional methods excluding the natural uncertainties of PV generation outputs and loads under the artificial uncertainties of LAAs, we propose a universal uncertainty-aware optimization framework into which both the natural and artificial uncertainties are incorporated simultaneously as shown in Fig. 1. The proposed DRO-based VVO framework contributes to resolving the natural uncertainties and LAAs on EVCS for a reliable and robust realistic three-phase unbalanced distribution system operation.
- *Exploitation of PV planning and curtailment in the DRO-based VVO model:* We incorporate the PV planning and curtailment processes into the DRO-based VVO problem. The added PV planning and curtailment functions aid to further mitigate the impact of the LAAs on distribution grid operations in the presence of the PV generation output and load uncertainties.
- *Tractable reformulation of the DRO-VVO problem:* We present tractable reformulations for the chance constraints of voltage magnitude, current magnitude, and curtailed PV real power in the PV planning/curtailment-integrated DRO problem. The DRO problem with the deterministic constraints obtained from the reformulation can be solved by off-the-shelf optimization solvers efficiently.
- *Performance validation of the DRO-based VVO method:* Simulation results obtained on IEEE 13-bus and 37-bus systems demonstrate the effectiveness of the proposed method in terms of optimization infeasibility, reduction of substation energy/voltage imbalance, PV deployment/curtailment, and solution conservatism along with sample efficiency.

In summary, this study proposes a PV planning/curtailment-integrated DRO-based VVO framework in the presence of the natural uncertainty and LAA on EVCS. Under uncertain and cyber attack environment, the integrated PV planning and curtailment processes aid to maintain stable distribution planning/operation with the minimized real power loss and voltage imbalance as well as mitigate the impact of LAA on EVCS through the real/reactive power dispatch of the PV systems. Given the parameters (e.g., distribution network parameter/topology/constraint, predicted PV/load/EVCS operation data based

on their historical data, and operational limits of PV systems), the proposed optimization framework calculates the values of decision variables (e.g., optimal location and size of PV systems, curtailed PV real generation outputs, and adjusted PV reactive power output). The proposed framework can potentially be used as a crucial uncertainty-aware application in distribution management system because it addresses both the natural uncertainties of PV generation outputs/loads and the artificial uncertainties of LAAs based on the DRO method by exploiting existing PV planning and curtailment methods.

The remaining paper is organized as follows. Section 2 introduces the system model with a linearized three-phase unbalanced distribution system. The attack and its mitigation strategy are described in Section 3. Section 4 presents the introduction and tractable reformulation of the DRO problem. Section 5 describes the simulation analysis for validating the proposed method, and Section 6 presents the concluding remarks.

2. System model

2.1. Notation

Bold symbols represent vectors or matrices. Hat symbols represent estimates of true parameter values. For an $N\times1$ complex vector $\mathbf{x}\in\mathbb{C}^N$, $\overline{\mathbf{x}}$ denotes the conjugate of $\mathbf{x}$, and diag($\mathbf{x}$) returns an $N\times N$ diagonal matrix with the elements of $\mathbf{x}$. j denotes an imaginary unit of the complex vector. $|\cdot|$ represents the absolute value of a number or vector or the cardinality of a set. $(\cdot)^\top$ represents the transpose of a vector.

2.2. Unbalanced distribution system model

For the set $\mathcal{N}$ of buses, consider a three-phase linear unbalanced AC distribution power flow model (Bazrafshan and Gatsis, 2018) with $|\mathcal{N}|$ buses having the following complex three-phase bus admittance matrix

$$\mathbf{Y}=\begin{bmatrix}\mathbf{Y}_{00} & \mathbf{Y}_{0L}\\ \mathbf{Y}_{L0} & \mathbf{Y}_{LL}\end{bmatrix}\in\mathbb{C}^{3(|\mathcal{N}|+1)\times3(|\mathcal{N}|+1)} \tag{1}$$

where $\mathbf{Y}_{00}\in\mathbb{C}^{3\times3}$, $\mathbf{Y}_{0L}\in\mathbb{C}^{3\times3|\mathcal{N}|}$, $\mathbf{Y}_{L0}\in\mathbb{C}^{3|\mathcal{N}|\times3}$, and $\mathbf{Y}_{LL}\in\mathbb{C}^{3|\mathcal{N}|\times3|\mathcal{N}|}$ are the submatrices of the admittance matrix including the substation. Based on the fixed-point linearization method, the linear models of the voltage, voltage magnitude, substation apparent power, and current at time t are expressed as (Bernstein and Dall'Anese, 2017)

$$\mathbf{v}_t=\mathbf{M}^Y\mathbf{x}_t^Y+\mathbf{M}^\Delta\mathbf{x}_t^\Delta+\mathbf{a} \tag{2}$$

$$|\mathbf{v}_t|=\mathbf{K}^Y\mathbf{x}_t^Y+\mathbf{K}^\Delta\mathbf{x}_t^\Delta+\mathbf{b} \tag{3}$$

$$\mathbf{s}_{s,t}=\mathbf{G}^Y\mathbf{x}_t^Y+\mathbf{G}^\Delta\mathbf{x}_t^\Delta+\mathbf{c} \tag{4}$$

$$\mathbf{i}_{ij,t}=\mathbf{J}_{ij}^Y\mathbf{x}_t^Y+\mathbf{J}_{ij}^\Delta\mathbf{x}_t^\Delta+\mathbf{d}_{ij}. \tag{5}$$

Here, $\mathbf{x}_t^{Y(\Delta)}=\left[\mathbf{p}_t^{\text{inj},Y(\Delta)\top},\mathbf{q}_t^{\text{inj},Y(\Delta)\top}\right]^\top$ represents the real ($\mathbf{p}_t^{\text{inj},Y(\Delta)}\in\mathbb{R}^{3|\mathcal{N}|}$) and reactive ($\mathbf{q}_t^{\text{inj},Y(\Delta)}\in\mathbb{R}^{3|\mathcal{N}|}$) power injection vectors with wye (delta) phase configuration at time t. The vectors $\mathbf{v}_t\in\mathbb{C}^{3|\mathcal{N}|}$ and $|\mathbf{v}_t|\in\mathbb{R}^{3|\mathcal{N}|}$ denote the complex voltages and voltage magnitudes for all buses and phases at time t, respectively. The apparent power at substation s is defined as $\mathbf{s}_{s,t}=\mathbf{p}_{s,t}+\mathrm{j}\mathbf{q}_{s,t}$ where $\mathbf{p}_{s,t},\mathbf{q}_{s,t}\in\mathbb{R}^3$ are the real and reactive power values at the substation at time t, respectively.

For a given power injection vector $\mathbf{s}=\left[(\mathbf{s}^Y)^\top,(\mathbf{s}^\Delta)^\top\right]^\top$, let $\widetilde{\mathbf{v}}$ and $\widetilde{\mathbf{s}}=\left[(\widetilde{\mathbf{s}}^Y)^\top,(\widetilde{\mathbf{s}}^\Delta)^\top\right]^\top$ represent the solution of the fixed-point equation (Bernstein et al., 2018). Then, consider the first iteration of the following fixed-point equation initiated at $\widetilde{\mathbf{v}}$:

$$\mathbf{v}=\mathbf{w}+\mathbf{Y}_{LL}^{-1}\left(\text{diag}(\overline{\widetilde{\mathbf{v}}})^{-1}\overline{\mathbf{s}^Y}+\mathbf{H}^\top\text{diag}(\mathbf{H}\overline{\widetilde{\mathbf{v}}})^{-1}\overline{\mathbf{s}^\Delta}\right) \tag{6}$$

where $\mathbf{w}=-\mathbf{Y}_{LL}^{-1}\mathbf{Y}_{L0}\mathbf{v}_0$ is the known zero-load voltage, $\mathbf{v}_0\in\mathbb{C}^3$ is the vector of substation voltages, and $\mathbf{H}$ is a $3(|\mathcal{N}|-1)\times3(|\mathcal{N}|-1)$ block-diagonal matrix where all diagonal submatrices are $[1\ \ -1\ 0;0\ \ 1\ \ -1;-1\ 0\ 1]$. Using $\mathbf{W}=\text{diag}(\mathbf{w})$ and the result (6), the parameter matrices and vectors for (2)–(4) can be written as follows:

$$\mathbf{M}^Y=(\mathbf{Y}_{LL}^{-1}\text{diag}(\overline{\widetilde{\mathbf{v}}})^{-1},-\mathrm{j}\mathbf{Y}_{LL}^{-1}\text{diag}(\overline{\widetilde{\mathbf{v}}})^{-1}) \tag{7}$$

$$\mathbf{M}^\Delta=(\mathbf{Y}_{LL}^{-1}\mathbf{H}^\top\text{diag}(\mathbf{H}\overline{\widetilde{\mathbf{v}}})^{-1},-\mathrm{j}\mathbf{Y}_{LL}^{-1}\mathbf{H}^\top\text{diag}(\mathbf{H}\overline{\widetilde{\mathbf{v}}})^{-1}) \tag{8}$$

$$\mathbf{a}=\mathbf{w} \tag{9}$$

$$\mathbf{K}^Y=|\mathbf{W}|\text{Re}\left\{\mathbf{W}^{-1}\mathbf{M}^Y\right\} \tag{10}$$

$$\mathbf{K}^\Delta=|\mathbf{W}|\text{Re}\left\{\mathbf{W}^{-1}\mathbf{M}^\Delta\right\} \tag{11}$$

$$\mathbf{b}=|\mathbf{w}| \tag{12}$$

$$\mathbf{G}^Y=\text{diag}(\mathbf{v_0})\overline{\mathbf{Y}}_{0L}\overline{\mathbf{M}}^Y \tag{13}$$

$$\mathbf{G}^\Delta=\text{diag}(\mathbf{v_0})\overline{\mathbf{Y}}_{0L}\overline{\mathbf{M}}^\Delta \tag{14}$$

$$\mathbf{c}=\text{diag}(\mathbf{v}_0)\left(\overline{\mathbf{Y}}_{00}\overline{\mathbf{v}}_0+\overline{\mathbf{Y}}_{0L}\overline{\mathbf{w}}\right). \tag{15}$$

To express the current, the phase impedance and shunt admittance matrices of the line spanning from bus i to j are defined as $\mathbf{Z}_{ij}\in\mathbb{C}^{3\times3}$ and $\mathbf{Y}_{ij}\in\mathbb{C}^{3\times3}$, respectively. The current vector $\mathbf{i}_{ij}=[i_{ij,a},i_{ij,b},i_{ij,c}]^\top$ of line ij is expressed as

$$\mathbf{i}_{ij}=\left[(\mathbf{Y}_{ij}+\mathbf{Z}_{ij}^{-1})\mathbf{E}_i-\mathbf{Z}_{ij}^{-1}\mathbf{E}_j\right]\mathbf{v} \tag{16}$$

where $\mathbf{E}_i=[\mathbf{0}_{3\times3(i-1)},\mathbf{I}_3,\mathbf{0}_{3\times3(|\mathcal{N}|-i)}]$. Given $\mathbf{B}_{ij}=\left[(\mathbf{Y}_{ij}+\mathbf{Z}_{ij}^{-1})\mathbf{E}_i-\mathbf{Z}_{ij}^{-1}\mathbf{E}_j\right]$, the parameter matrices and vector for (5) can be obtained using (2) and (16) as follows:

$$\mathbf{J}_{ij}^Y=\mathbf{B}_{ij}\mathbf{M}^Y,\ \mathbf{J}_{ij}^\Delta=\mathbf{B}_{ij}\mathbf{M}^\Delta,\ \mathbf{d}_{ij}=\mathbf{B}_{ij}\mathbf{w}. \tag{17}$$

2.3. VVO model

In this subsection, all the variables and parameters for the VVO model are represented by the elements of their corresponding vectors. Let us define the set of buses as $\mathcal{N}$. The set $\mathcal{N}$ includes the following three subsets: (i) $\mathcal{N}^{\text{PV}}$ for PV systems, (ii) $\mathcal{N}^{\text{L}}$ for loads, and (iii) $\mathcal{N}^{\text{EVCS}}$ for EVCSs. Therefore, the indices i, p, l, and E represent the locations of the buses ($i\in\mathcal{N}$), PV systems ($p\in\mathcal{N}^{\text{PV}}$), loads ($l\in\mathcal{N}^{\text{L}}$), and EVCSs ($E\in\mathcal{N}^{\text{EVCS}}$), respectively, where $\mathcal{N}^{\text{PV}},\mathcal{N}^{\text{L}},\mathcal{N}^{\text{EVCS}}\subseteq\mathcal{N}$. The index ϕ represents the phase $\phi\in\boldsymbol{\Phi}:=\{a,b,c\}$.

2.3.1. Operating constraints

For each phase ϕ and time t with the $Y(\Delta)$ phase configuration, constraint (18) corresponds to the real power injection ($p_{i,\phi,t}^{\text{inj},Y(\Delta)}$) at bus i, which consists of the predicted PV real power generation output ($\hat{p}_{p,\phi,t}^{\text{PV}}$) at bus p, predicted real power load demand ($\hat{p}_{l,\phi,t}^{\text{load}}$) at bus l, and predicted aggregated EV real charging power ($\hat{p}_{E,\phi,t}^{\text{EVCS}}$) at bus E. Constraint (19) corresponds to the reactive power injection ($q_{i,\phi,t}^{\text{inj},Y(\Delta)}$) at bus i, which consists of the reactive power ($q_{p,\phi,t}^{\text{PV}}$) of the PV system at bus p and predicted reactive power load demand ($\hat{q}_{l,\phi,t}^{\text{load}}$) at bus l. The ranges of admissible voltages and currents for all buses and lines are expressed in (20)–(21). According to (21), the real part of the complex current ($i_{ij,\phi,t}$) must be below its maximum limit Re($i_{ij,t}^{\max}$). We set the power factor of the current limit as 0.9 to ensure that the real part of the current limit can be parameterized, thereby facilitating the formulation of a tractable DRO problem along with current limit constraints. Details regarding the current limit for an AC system considering the apparent power can be found in Andrianesis et al. (2022).

$$p_{i,\phi,t}^{\text{inj},Y(\Delta)}=\hat{p}_{p,\phi,t}^{\text{PV}}-\hat{p}_{l,\phi,t}^{\text{load}}-\hat{p}_{E,\phi,t}^{\text{EVCS}} \tag{18}$$

$$q_{i,\phi,t}^{\text{inj},Y(\Delta)}=q_{p,\phi,t}^{\text{PV}}-\hat{q}_{l,\phi,t}^{\text{load}} \tag{19}$$

$$\upsilon^{\min}\le|v_{i,\phi,t}|\le\upsilon^{\max} \tag{20}$$

$$-\text{Re}(i_{ij,t}^{\max})\le\text{Re}(i_{ij,\phi,t})\le\text{Re}(i_{ij,t}^{\max}). \tag{21}$$

Constraint (22) limits the reactive power ($q^{\mathrm{PV}}_{p,\phi,t}$) of the PV system at bus p using its apparent power ($s^{\mathrm{PV}}_{p,\phi}$) and the maximum real power ($p^{\mathrm{PV,max}}_{p,\phi,t}$). For the reduction of computation complexity, the predicted values of PV generation output ($\hat{p}^{\mathrm{PV}}_{p,\phi,t}$), and real (reactive) load ($\hat{p}(\hat{q})^{\mathrm{load}}_{l,\phi,t}$) are calculated via the average of their corresponding historical data using open datasets (IEEE-PES, 2015). The total predicted charging demand ($\hat{p}^{\mathrm{EVCS}}_{E,\phi,t}$) of EVs at EVCS is calculated as the sum of randomly generated charging powers of individual EVs using (26) and EV dataset (Wu et al., 2010).

$$(p^{\mathrm{PV,max}}_{p,\phi,t})^2 + (q^{\mathrm{PV}}_{p,\phi,t})^2 \le (s^{\mathrm{PV}}_{p,\phi})^2. \tag{22}$$

2.3.2. Objective function

For each phase $\phi \in \Phi$ and time $t \in \mathcal{T}$, the DSO conducts VVO by minimizing the weighted multi-objective function $\mathcal{J}^{\mathrm{VVO}}$ (23) with positive weights ω_1 and ω_2.

$$\mathcal{J}^{\mathrm{VVO}} = \omega_1 J_1 + \omega_2 J_2 \tag{23}$$

$$J_1 = \sum_{t\in\mathcal{T}} \sum_{\phi\in\Phi} p_{s,\phi,t} \tag{24}$$

$$J_2 = \sum_{t\in\mathcal{T}} \sum_{i\in\mathcal{N}} ||v_{i,a,t}| - |v_{i,b,t}|| + ||v_{i,b,t}| - |v_{i,c,t}|| + ||v_{i,c,t}| - |v_{i,a,t}|| \tag{25}$$

where J_1 and J_2 in (24) and (25) denote the total real power flow at the substation for the three phases and the total voltage imbalance among the three phases for all buses during the entire scheduling period $|\mathcal{T}|$, respectively.

3. LAA on EVCS and mitigation strategy

3.1. Statement of load altering attack problem

The DSO performs inverter-based VVO in an unbalanced three-phase distribution system with PV systems and EVCSs. The VVO controls the reactive powers of the PV systems via their smart inverters to minimize the total real power flow at the substation and total voltage imbalance among the three phases for all buses during the scheduling period. We consider a situation in which the LAA distorts the controllable loads (i.e., the charging of EVs at EVCSs) by directly manipulating their charging control signals.

For EV $e \in \mathcal{N}^{\mathrm{EVCS}}_{E}$ at EVCS $E \in \mathcal{N}^{\mathrm{EVCS}}$ and time t, the total predicted charging demand $\hat{p}^{\mathrm{EVCS}}_{E,\phi,t}$ of EVs in (18) can be expressed as

$$\hat{p}^{\mathrm{EVCS}}_{E,\phi,t} = \sum_{e\in\mathcal{N}^{\mathrm{EVCS}}_{E}} \hat{x}^{\mathrm{EV}}_{e,t} \hat{p}^{\mathrm{EV}}_{e,t} \tag{26}$$

where $\hat{p}^{\mathrm{EV}}_{e,t}$ is a sampled random EV charging power, and $\hat{x}^{\mathrm{EV}}_{e,t}$ is a binary EV charging control signal that determines the status of EV charging (i.e., "1" for charging and "0" for non-charging). Given the total EV charging demand (26), the LAAs can be categorized into the following two types:

- Type A attack: Changes the EV charging status from $\hat{x}^{\mathrm{EV}}_{e,t} = 0$ to $\hat{x}^{\mathrm{EV}}_{e,t} = 1$.
- Type B attack: Changes the EV charging status from $\hat{x}^{\mathrm{EV}}_{e,t} = 1$ to $\hat{x}^{\mathrm{EV}}_{e,t} = 0$.

Type A attacks may result in line overloading and voltage lower limit violation with high voltage drop owing to an increase in the EV charging demand. In contrast, Type B attacks may decrease the EV charging demand, leading to undesirable load reduction. Furthermore, Type B attacks can indirectly cause the PV system to control its real and reactive power supplies differently and resort to a higher real power curtailment. These detrimental impacts of Type A (or Type B) attacks are aggravated when the distribution system has a high (or low) PV penetration with low (or high) load demand. The charging demand and status of the EV are considered to be stochastic in this analysis, and the data are generated from a dataset.

3.2. PV planning and curtailment-based attack mitigation

This section presents the LAA-mitigation strategy through which the DSO performs PV planning and curtailment aimed at determining optimal location and size of the PV systems and PV generation outputs, respectively.

To formulate the VVO problem integrated with the PV planning and curtailment-based attack mitigation strategy, constraint (22) associated with the reactive power capability of PV systems is rewritten as follows:

$$p^{\mathrm{PV}}_{p,\phi,t} + p^{\mathrm{PV,c}}_{p,\phi,t} = p^{\mathrm{PV,max}}_{p,\phi,t} \tag{27}$$

$$p^{\mathrm{PV,max}}_{p,\phi,t} = u^{\mathrm{PV}}_{p,t} s^{\mathrm{PV}}_{p,\phi} \tag{28}$$

$$p^{\mathrm{PV,c}}_{p,\phi,t} \le \gamma p^{\mathrm{PV,max}}_{p,\phi,t} \tag{29}$$

$$(p^{\mathrm{PV}}_{p,\phi,t})^2 + (q^{\mathrm{PV}}_{p,\phi,t})^2 \le (s^{\mathrm{PV}}_{p,\phi})^2 \tag{30}$$

$$-\psi s^{\mathrm{PV}}_{p,\phi} \le q^{\mathrm{PV}}_{p,\phi,t} \le \psi s^{\mathrm{PV}}_{p,\phi} \tag{31}$$

$$s^{\mathrm{PV}}_{p,\phi} = \hat{s}^{\mathrm{PV}}_{p,\phi} + s^{\mathrm{PV,+}}_{p,\phi} \tag{32}$$

$$0 \le s^{\mathrm{PV,+}}_{p,\phi} \le s^{\mathrm{PV,+,max}}(z_p + \hat{z}_p). \tag{33}$$

Constraint (27) represents the maximum real power ($p^{\mathrm{PV,max}}_{p,\phi,t}$) of PV system p at phase ϕ and time t, which consists of the real power ($p^{\mathrm{PV}}_{p,\phi,t}$) and curtailed real power ($p^{\mathrm{PV,c}}_{p,\phi,t}$) of the PV system. The maximum PV real power is expressed as a percentage ($u^{\mathrm{PV}}_{p,t}$) of the maximum irradiance of the PV capacity ($s^{\mathrm{PV}}_{p,\phi}$) in (28) where $0 \le u^{\mathrm{PV}}_{p,t} \le 1$. Constraint (29) limits the curtailed PV real power ($p^{\mathrm{PV,c}}_{p,\phi,t}$), which is described in terms of the maximum PV real power ($p^{\mathrm{PV,max}}_{p,\phi,t}$) and its coefficient ($0 \le \gamma \le 1$). Constraints (30) and (31) restrict the capacity and reactive power ($q^{\mathrm{PV}}_{p,\phi,t}$) of the PV system with $0 \le \psi \le 1$, respectively. The capacity of PV system is expressed as the sum of the existing PV capacity ($\hat{s}^{\mathrm{PV}}_{p,\phi}$) and newly added PV capacity ($s^{\mathrm{PV,+}}_{p,\phi}$) in (32). The added PV capacity is limited in (33) where $\hat{z}_p$ is a binary parameter for the location of the existing PV system and z_p is a binary variable that determines the optimal location of the new PV system. $s^{\mathrm{PV,+,max}}$ is the maximum additional PV capacity.

Next, the weighted multi-objective function $\mathcal{J}^{\mathrm{VVO\text{-}PC}}$ (34) with positive weights ω_3 and ω_4 is added to $\mathcal{J}^{\mathrm{VVO}}$ (23) to minimize the installation and capacity upgrade costs (J_3) of PV systems and curtailment cost (J_4) of the PV generation output:

$$\mathcal{J}^{\mathrm{VVO\text{-}PC}} = \omega_3 J_3 + \omega_4 J_4 \tag{34}$$

$$J_3 = \sum_{\phi\in\Phi} \sum_{p\in\mathcal{N}^{\mathrm{PV}}} \pi_1 z_p + \pi_2 s^{\mathrm{PV,+}}_{p,\phi} \tag{35}$$

$$J_4 = \sum_{t\in\mathcal{T}} \sum_{\phi\in\Phi} \sum_{p\in\mathcal{N}^{\mathrm{PV}}} \pi_3 p^{\mathrm{PV,c}}_{p,\phi,t} \tag{36}$$

where π_1 and π_2 in (35) are the prices for the PV system installation and capacity upgrade, respectively, and π_3 in (36) is the price for the PV generation output curtailment.

4. DRO PROBLEM formulation

A DRO problem is formulated for the DSO to maintain stable power distribution operations through PV system installment/capacity upgrade and PV real power curtailment in scenarios involving LAAs on EVCSs under uncertainties in the PV generation outputs and loads. Using an ambiguity set based on the Wasserstein metric (Section 4.1), the chance constraints of voltage/current magnitude and curtailed PV real power due to uncertain PV generation outputs and loads are formulated (Section 4.2). Subsequently, tractable reformulations of the chance constraints are presented (Section 4.3).

4.1. Ambiguity set based on the wasserstein metric

To evaluate the inherent uncertainty in PV generation outputs and loads, the following Wasserstein metric of two probability distributions $\mathbb{P}_1, \mathbb{P}_2 \in \mathcal{M}(\Xi)$ is defined:

$$d_W(\mathbb{P}_1, \mathbb{P}_2) := \inf\left\{ \int_{\Xi^2} \|\xi_1 - \xi_2\| \mathbb{Q}(d\xi_1, d\xi_2) \right\} \tag{37}$$

where $\mathbb{Q}$ denotes a joint distribution of two random vectors ξ_1 and ξ_2 with marginal distributions $\mathbb{P}_1$ and $\mathbb{P}_2$, $\mathcal{M}(\Xi)$ represents a probability space containing all probability distributions $\mathbb{P}$ supported on the uncertainty set Ξ, and $\|\cdot\|$ indicates an arbitrary norm.

Using the Wasserstein metric (37), an ambiguity set $\mathcal{P}_N(\delta)$ is constructed, which is expressed as a Wasserstein ball of radius δ centered at the empirical distribution $\widehat{\mathbb{P}}_N$:

$$\mathcal{P}_N(\delta) = \left\{ \mathbb{P} \in \mathcal{M}(\Xi) : d_W(\widehat{\mathbb{P}}_N, \mathbb{P}) \le \delta \right\} \tag{38}$$

In (38), the empirical distribution $\widehat{\mathbb{P}}_N$ is constructed with N historical samples $\widehat{\xi}_i$:

$$\widehat{\mathbb{P}}_N := \frac{1}{N} \sum_{i=1}^{N} \delta_{\widehat{\xi}_i} \tag{39}$$

where $\delta_{\widehat{\xi}_i}$ represents the unit point mass at $\widehat{\xi}_i$.

4.2. Chance constraints

In the presence of uncertain PV generation outputs and loads, the deterministic constraints for voltage magnitude (20), current magnitude (21), and curtailed PV real power (29) can be transformed into the following chance constraints:

$$\inf_{\mathbb{P}\in\mathcal{P}_N(\delta)} \mathbb{P}\left\{ v^{\min} \le |v_{i,\phi,t}| \right\} \ge 1-\beta \tag{40}$$

$$\inf_{\mathbb{P}\in\mathcal{P}_N(\delta)} \mathbb{P}\left\{ |v_{i,\phi,t}| \le v^{\max} \right\} \ge 1-\beta \tag{41}$$

$$\inf_{\mathbb{P}\in\mathcal{P}_N(\delta)} \mathbb{P}\left\{ -\mathrm{Re}(i_{ij,t}^{\max}) \le \mathrm{Re}(i_{ij,t}) \right\} \ge 1-\beta \tag{42}$$

$$\inf_{\mathbb{P}\in\mathcal{P}_N(\delta)} \mathbb{P}\left\{ \mathrm{Re}(i_{ij,t}) \le \mathrm{Re}(i_{ij,t}^{\max}) \right\} \ge 1-\beta \tag{43}$$

$$\inf_{\mathbb{P}\in\mathcal{P}_N(\delta)} \mathbb{P}\left\{ p_{p,\phi,t}^{\mathrm{PV,c}} \le \gamma p_{p,\phi,t}^{\mathrm{PV,max}} \right\} \ge 1-\beta. \tag{44}$$

According to these chance constraints, with a minimum probability of $1-\beta$ under the worst-case probability distribution $\mathbb{P}$ within the ambiguity set $\mathcal{P}_N(\delta)$, the voltage magnitude $|v_{i,\phi,t}|$ must be within its allowable range in (40) and (41), and the real current magnitude and curtailed PV real power must be less than or equal to the current limit in (42) and (43) and scaled maximum real power output (44) of the PV system, respectively.

4.3. Reformulation of the chance constraints

For the Wasserstein-metric-based DRO problem, a general form for the feasible set of the chance constraints (40)–(44) can be expressed as

$$\inf_{\mathbb{P}\in\mathcal{P}_N(\delta)} \mathbb{P}\left\{ \xi : \mathbf{a}(\mathbf{x})^\top \xi_k \le \mathbf{b}_k(\mathbf{x}), \forall k \in \mathcal{K} \right\} \ge 1-\beta. \tag{45}$$

Here, $\mathbf{x}$ is the vector of decision variables. ξ_k is the random vector supported on the uncertainty set Ξ_k where $k \in \mathcal{K}$ is the index of constraints. $\mathbf{a}(\mathbf{x}) = (\eta_1 \mathbf{x}, \eta_2)^\top$ is the affine function of $\mathbf{x}$ with parameters η_1 and η_2, which includes the random variables. The function $\mathbf{b}_k(\mathbf{x})$ does not have random variables.

For a tractable reformulation of the chance constraints, the feasible set can be transformed into the following mixed-integer form based on optimization methods including the strong duality theorem, conditional-value-at-risk notion, and big-M method (See Corollary 1 and Proposition 1 (Xie, 2019)):

$$\delta\nu - \beta\kappa \le \frac{1}{N}\sum_{j=1}^{N} z_j \tag{46}$$

$$z_j + \kappa \le s_j \tag{47}$$

$$s_j \le b_k(\mathbf{x}) - \mathbf{a}(\mathbf{x})^\top \widehat{\xi}_{j,k} + M_j(1-y_j) \tag{48}$$

$$s_j \le M_j y_j \tag{49}$$

$$\|\mathbf{a}(\mathbf{x})\|_* \le \nu \tag{50}$$

$$\nu > 0, \kappa \ge 0, s_j \ge 0, z_j \le 0, y_j \in \{0,1\}. \tag{51}$$

Here, $\widehat{\xi}_{j,k}$ is the jth sample of the random vector at constraint k, from a sample set $\{\widehat{\xi}_{1,k}, \widehat{\xi}_{2,k}, \ldots, \widehat{\xi}_{N,k}\}$; ν, κ, s_j, z_j and y_j are auxiliary variables; M_j is a big-M coefficient; $\|\mathbf{a}(\mathbf{x})\|_*$ represents the L-1 or L-inf norm for the linear programming form and L-2 norm for the second-order cone programming form.

We consider two types of random vectors, ξ^{PV} and ξ^{load}, which correspond to the PV generation outputs and loads, respectively. The chance constraints (40)–(44) can be transformed into the deterministic constraints (46)–(51) using the samples of the random vectors.

A key part of this transformation is to construct the inequality constraint (48). For the constraint (44), we start with the deterministic constraint $p_{p,\phi,t}^{\mathrm{PV,c}} \le \gamma p_{p,\phi,t}^{\mathrm{PV,max}}$. In (28), we replace $u_{p,t}^{\mathrm{PV}}$ by the sample $\widehat{\xi}_{p,j}^{\mathrm{PV}}$ of the random variable to derive the following constraint:

$$s_j \le -p_{p,\phi,t}^{\mathrm{PV,c}} + \gamma s_{p,\phi}^{\mathrm{PV}} \widehat{\xi}_{p,j}^{\mathrm{PV}} + M_j(1-y_j). \tag{52}$$

Similarly, using the sample $\widehat{\xi}_{l,j}^{\mathrm{load}}$ of the random variable for the load, each inequality constraint (48) for the chance constraints (40)–(43) is derived as follows:

$$\begin{aligned} s_j \le & -|v^{\min}| + \mathbf{w}_m + \mathbf{K}_m^{Y(\Delta)}((-\widehat{\mathbf{p}}_E^{\mathrm{EVCS}} - \mathbf{p}_p^{\mathrm{PV,c}})^\top, (\mathbf{q}_p^{\mathrm{PV}})^\top)^\top \\ & + \mathbf{K}_m^{Y(\Delta)}((-\widehat{\xi}_{p,j}^{\mathrm{PV}}\mathbf{s}_p^{\mathrm{PV}})^\top, (\mathbf{0}_{3|\mathcal{N}|})^\top)^\top \\ & + \mathbf{K}_m^{Y(\Delta)}((-\widehat{\xi}_{l,j}^{\mathrm{load}}\mathbf{p}_l^{\mathrm{load,nom}})^\top, (\mathbf{0}_{3|\mathcal{N}|})^\top)^\top \\ & + \mathbf{K}_m^{Y(\Delta)}((\mathbf{0}_{3|\mathcal{N}|})^\top, (-\widehat{\xi}_{l,j}^{\mathrm{load}}\mathbf{q}_l^{\mathrm{load,nom}})^\top)^\top + M_j(1-y_j) \end{aligned} \tag{53}$$

$$\begin{aligned} s_j \le & |v^{\max}| - \mathbf{w}_m - \mathbf{K}_m^{Y(\Delta)}((-\widehat{\mathbf{p}}_E^{\mathrm{EVCS}} - \mathbf{p}_p^{\mathrm{PV,c}})^\top, (\mathbf{q}_p^{\mathrm{PV}})^\top)^\top \\ & - \mathbf{K}_m^{Y(\Delta)}((-\widehat{\xi}_{p,j}^{\mathrm{PV}}\mathbf{s}_p^{\mathrm{PV}})^\top, (\mathbf{0}_{3|\mathcal{N}|})^\top)^\top \\ & - \mathbf{K}_m^{Y(\Delta)}((-\widehat{\xi}_{l,j}^{\mathrm{load}}\mathbf{p}_l^{\mathrm{load,nom}})^\top, (\mathbf{0}_{3|\mathcal{N}|})^\top)^\top \\ & - \mathbf{K}_m^{Y(\Delta)}((\mathbf{0}_{3|\mathcal{N}|})^\top, (-\widehat{\xi}_{l,j}^{\mathrm{load}}\mathbf{q}_l^{\mathrm{load,nom}})^\top)^\top + M_j(1-y_j) \end{aligned} \tag{54}$$

$$\begin{aligned} s_j \le & -\mathrm{Re}(i_{ij,m}^{\max}) + \mathrm{Re}\{d_{ij,m}\} \\ & + \mathrm{Re}\{\mathbf{J}_{ij,m}^{Y(\Delta)}((-\widehat{\mathbf{p}}_E^{\mathrm{EVCS}} - \mathbf{p}_p^{\mathrm{PV,c}})^\top, (\mathbf{q}_p^{\mathrm{PV}})^\top)^\top \\ & + \mathbf{J}_{ij,m}^{Y(\Delta)}((-\widehat{\xi}_{p,j}^{\mathrm{PV}}\mathbf{s}_p^{\mathrm{PV}})^\top, (\mathbf{0}_{3|\mathcal{N}|})^\top)^\top \\ & + \mathbf{J}_{ij,m}^{Y(\Delta)}((-\widehat{\xi}_{l,j}^{\mathrm{load}}\mathbf{p}_l^{\mathrm{load,nom}})^\top, (\mathbf{0}_{3|\mathcal{N}|})^\top)^\top \\ & + \mathbf{J}_{ij,m}^{Y(\Delta)}((\mathbf{0}_{3|\mathcal{N}|})^\top, (+\widehat{\xi}_{l,j}^{\mathrm{load}}\mathbf{q}_l^{\mathrm{load,nom}})^\top)^\top\} + M_j(1-y_j) \end{aligned} \tag{55}$$

$$\begin{aligned} s_j \le & \mathrm{Re}(i_{ij,m}^{\max}) - \mathrm{Re}\{d_{ij,m}\} \\ & - \mathrm{Re}\{\mathbf{J}_{ij,m}^{Y(\Delta)}((-\widehat{\mathbf{p}}_E^{\mathrm{EVCS}} - \mathbf{p}_p^{\mathrm{PV,c}})^\top, (\mathbf{q}_p^{\mathrm{PV}})^\top)^\top \\ & - \mathbf{J}_{ij,m}^{Y(\Delta)}((-\widehat{\xi}_{p,j}^{\mathrm{PV}}\mathbf{s}_p^{\mathrm{PV}})^\top, (\mathbf{0}_{3|\mathcal{N}|})^\top)^\top \\ & - \mathbf{J}_{ij,m}^{Y(\Delta)}((-\widehat{\xi}_{l,j}^{\mathrm{load}}\mathbf{p}_l^{\mathrm{load,nom}})^\top, (\mathbf{0}_{3|\mathcal{N}|})^\top)^\top \\ & - \mathbf{J}_{ij,m}^{Y(\Delta)}((\mathbf{0}_{3|\mathcal{N}|})^\top, (-\widehat{\xi}_{l,j}^{\mathrm{load}}\mathbf{q}_l^{\mathrm{load,nom}})^\top)^\top\} + M_j(1-y_j) \end{aligned} \tag{56}$$

where m is the index of the mth row of the matrix. The uncertainty of the deterministic load $\mathbf{p}(\mathbf{q})_l^{\mathrm{load}}$ is characterized by the product of its nominal value $\mathbf{p}(\mathbf{q})_l^{\mathrm{load,nom}}$ and the sample $\widehat{\xi}_{l,j}^{\mathrm{load}}$ of the random variable.

Finally, the proposed DRO problem is formulated as follows:

$$\min \mathcal{J}^{\mathrm{VVO}} + \mathcal{J}^{\mathrm{VVO\text{-}PC}} \tag{57}$$

s.t.

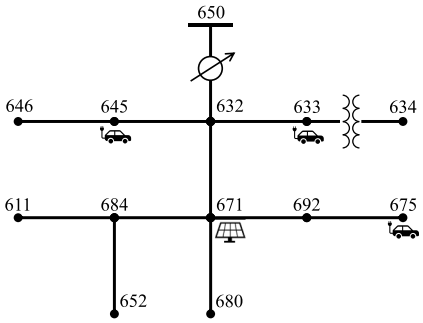

Fig. 2. IEEE 13-bus system with one PV system and three EVCSs.

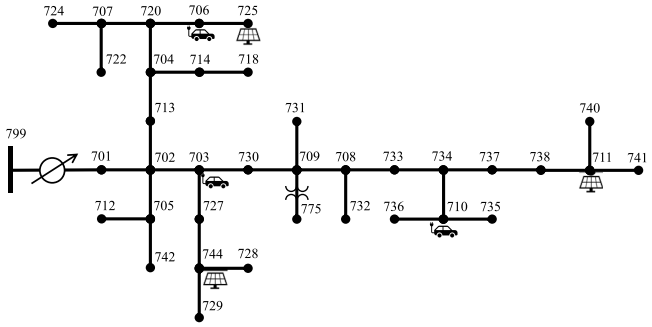

Fig. 3. IEEE 37-bus system with three PV systems and three EVCSs.

Power flow constraints : (3)–(5), (7)–(15), (17) (58)

PV/EVCS operational constraints : (18), (19), (26) (59)

PV planning/curtailment constraints : (28), (30)–(33) (60)

Tractable constraints: (46)–(56). (61)

5. Numerical examples

5.1. Simulation setup

The performance of the proposed framework was quantified over unbalanced IEEE 13-bus and 37-bus systems, as shown in Figs. 2 and 3, respectively. For both systems, the profiles of PV generation outputs and loads were extracted from open datasets with data for three months (IEEE-PES, 2015), as shown in Figs. 4(a) and 4(b). For the IEEE 13-bus system, one PV system with a capacity of 200 kVA was installed at bus 671. Three EVCSs were connected to buses 633, 645, and 675 with and each EVCS having 40 charging poles with a maximum charging power of 8 kW. For the IEEE 37-bus system, three PV systems with a capacity of 150 kVA were installed at buses 711, 725, and 744. Three EVCSs were connected to buses 703, 706, and 710 with each EVCS having 80 charging poles with a maximum charging power of 8 kW. 1000 data samples associated with the charging behavior of EVs were generated using the National Travel Survey datasets (Wu et al., 2010) for the driving distributions of weekdays. The number of EVs for three EVCSs at each time step are presented in Fig. 5. The base apparent power and voltage in the IEEE 13-bus and 37-bus system are set to {5 MVA, 4.16 kV} and {2.5 MVA, 4.8 kV}, respectively.

The weights of the multi-objective function (57) were set as $\{\omega_1 = 10, \omega_2 = 0.5, \omega_3 = 1.2, \omega_4 = 2\}$. For the objective functions J_3 (35) and J_4 (36), the prices for the installation, capacity upgrade, and curtailment of the PV system were set as $\{\pi_1 = \$20\text{K}, \pi_2 = \$1\text{K/kVA}, \pi_3 = \$10\text{/kWh}\}$, respectively. The minimum and maximum voltage magnitude limits were set as $v^{\min} = 0.95$ p.u. and $v^{\max} = 1.05$ p.u., respectively. The limits for the PV curtailment and PV reactive power were set as $\gamma = 0.2$ and $\psi = 0.8$, respectively. The values of the nominal loads and current limits were obtained from OpenDSS. The parameters for the DRO problem were set as follows: $\beta = 0.05$, $N = 20$, and $\delta = 1$. The big-M coefficient was set as $M = 1000$.

Table 1
Case classification.

Optimization method	Case number	Planning addition	Attack occurrence
DO	Case 1	No	No
	Case 2		Yes
DRO	Case 3	No	No
	Case 4		Yes
	Case 5	Yes	No
	Case 6		Yes

Table 2
Percentage of voltage and current violations in the IEEE 13-bus system for Cases 1 and 2.

Case	1	2-1 (bus 633)	2-2 (bus 645)
Voltage violation (%)	0	2.11	2.96
Current violation (%)	0	4.72	7.17

Table 1 classifies the six cases designed for the simulation study. Cases 1 and 2 correspond to DO methods with only the objective function $\mathcal{J}^{\text{VVO}}$ (i.e., no PV planning) in scenarios not involving and involving LAAs, respectively. Cases 3–6 represent the DRO methods that manage the uncertainties in the PV generation outputs and loads. In terms of planning with the objective function $\mathcal{J}^{\text{VVO-PC}}$ and its corresponding constraints, the aforementioned four cases are categorized into two groups: {Case 3, Case 4} without the planning stage and {Case 5, Case 6} with the planning stage. Each group is divided into two cases based on the existence of the LAA. The LAAs may occur simultaneously on various EV chargers in the EVCSs during the entire scheduling period. In addition, the LAAs are assumed to attack 20% randomly selected from all charging poles in the EVCSs at each time step. The proportion of Type A and Type B attacks are randomly calculated using the Gaussian distribution. The proposed strategy was simulated in a computer with an AMD Ryzen 7 2700X Processor clocked at 3.7 GHz and 32 GB of RAM using the YALMIP optimization tool with Gurobi 9.0 solver through MATLAB R2022a.

5.2. Comparison of simulation results for the six cases

5.2.1. Case 1 vs. Case 2

This comparison highlights the impact of the LAAs at buses 633 and 645 on the voltage and current violations of the DO-based VVO problem. The worst-case scenario involving the maximum PV generation outputs under 1000 random scenarios is considered, which increases the voltage level above its lower limit. When the VVO problem yields an infeasible solution with the voltage and current violations, a distribution load flow problem is solved using OpenDSS.

Table 2 compares the voltage and current violations in the IEEE 13-bus system between Cases 1 and 2. The voltage and current violations represent the percentage of the number of buses and lines with voltage and current violations with respect to the total number of buses and lines in 1000 random scenarios, respectively. Figs. 6 and 7 show the probabilities of voltage and current violations for all buses and phases under LAAs at buses 633 and 645, respectively. Note from Table 2 and these figures that the LAAs generate significant voltage and current violation via the distortion of EVs charging at EVCSs. These observations motivate us to develop LAA-mitigation strategy using the DRO method, which alleviates the LAA-induced constraint violations while addressing the various uncertainties in power distribution systems.

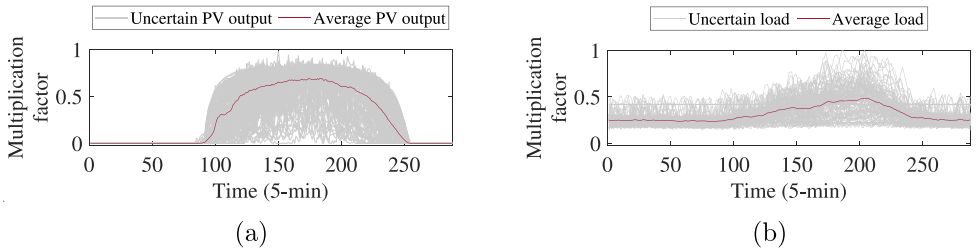

Fig. 4. Actual and average profiles of (a) PV generation output and (b) load.

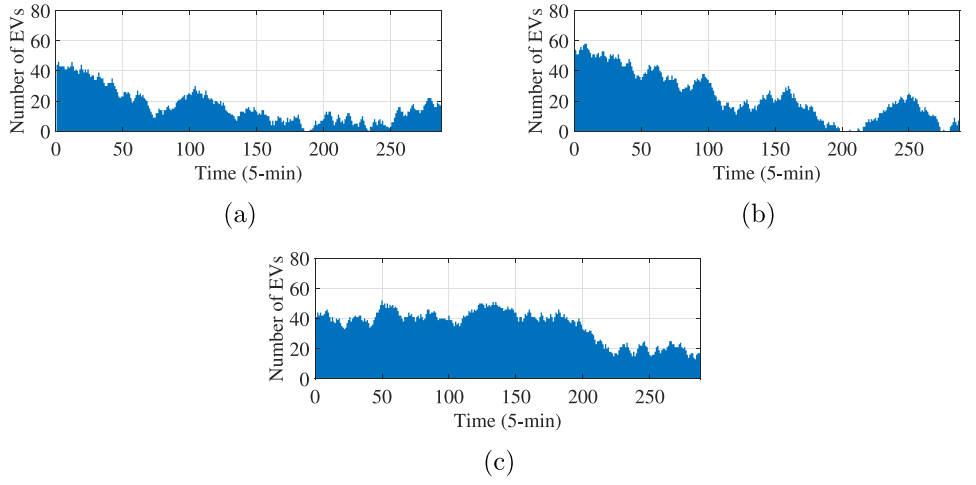

Fig. 5. Number of EVs during the entire scheduling period at: (a) EVCS1, (b) EVCS2, and (c) EVCS3.

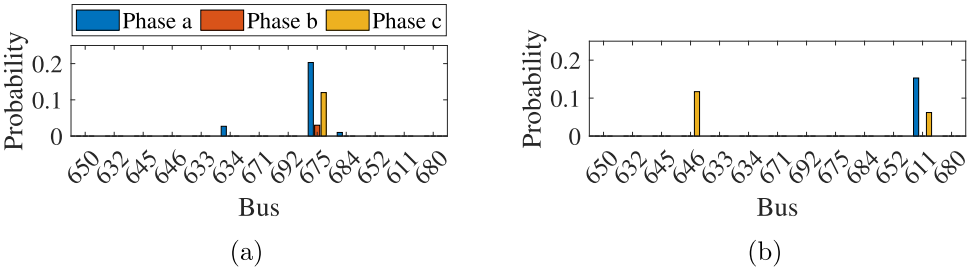

Fig. 6. Probability of voltage violations in the IEEE 13-bus system: (a) LAA at bus 633 and (b) LAA at bus 645.

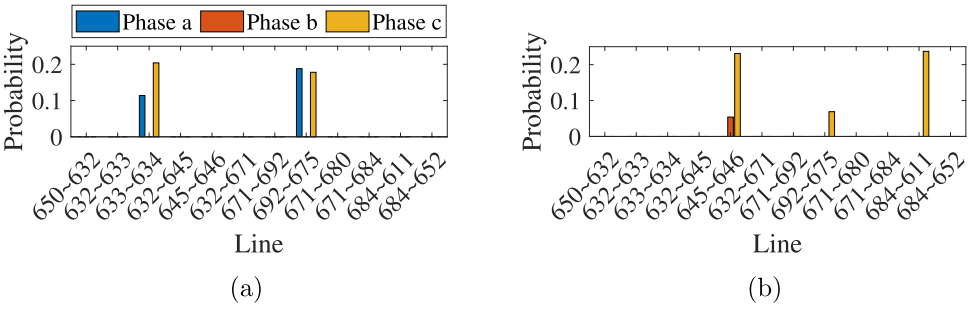

Fig. 7. Probability of current violations in the IEEE 13-bus system: (a) LAA at bus 633 and (b) LAA at bus 645.

5.2.2. Case 3 vs. Case 4

Table 3 presents the values of the total real power flow (J_1) at the substation and total voltage imbalance (J_2) for Cases 3 and 4 using the DRO method without PV planning. Unlike the DO method used in Cases 1 and 2, the method used in Cases 3 and 4 resolves the solution infeasibility issue under the LAAs along with uncertainty in the PV generation outputs and loads. However, as shown in Table 3, the LAAs at buses 633 and 645 increase the substation real power and voltage

Table 3
Performance comparison for Cases 3 and 4 of the IEEE 13-bus system.

Case	3	4-1 (bus 633)	4-2 (bus 645)
Substation energy J_1 (MWh)	572.81	608.29	605.95
Voltage imbalance J_2 (p.u)	74.46	76.07	75.79

Table 4
Performance comparison for Cases 5 and 6 of the IEEE 13-bus system.

Case	5		6-1 (bus 633)		6-2 (bus 645)	
Substation energy J_1 (MWh)	483.42		485.39		484.26	
Voltage imbalance J_2 (p.u)	61.17		62.78		62.5	
PV deployment cost J_3 (K$)	141		139		136	
PV curtailment cost J_4 ($)	204		239		223	
PV location	671	645	671	633	671	645
PV capacity (kVA)	225	96	227	92	227	89
PV curtailment (%)	0.4	3.8	1.2	8.1	0.9	9.2

Table 5
Average substation energies and total PV costs associated with the RO, DRO, and SO methods in the IEEE 13-bus system.

Method	RO	DRO	SO
Substation energy (MWh)	512.69	484.26	468.39
Total PV cost ($)	167,599	136,223	125,316

imbalance by {6.19%, 2.16%} and {5.78%, 1.78%}, respectively. These detrimental effects must be reduced to ensure stable and economical distribution system operations.

5.2.3. Case 5 vs. Case 6

Table 4 presents the results of Cases 5 and 6 that use the proposed DRO method with the planning stage. Compared with those in Cases 3 and 4, the real power flow at the substation and voltage imbalance for Cases 5 and 6 decrease significantly owing to the addition of the planning stage. However, the added planning stage incurs the PV deployment cost (J_3) (i.e., the sum of the costs for PV installation and capacity upgrade) and curtailment cost (J_4) associated with the existing and newly added PV systems.

Table 4 indicates that the new PV systems for Cases 6–1 and 6–2 are installed at buses 633 and 645, respectively, and their capacities are smaller than those for Case 5, which decreases the PV deployment cost. In contrast, Cases 6–1 and 6–2 have higher PV curtailment costs than those in Case 5. These results are attributable to the fact that the PV systems with the reduced capacity and high curtailment of PV generation outputs prevent over-and undervoltage/current violations. Moreover, the locations of the new PV systems for Cases 6–1 and 6–2 are consistent with the buses attacked by the LAAs, which mitigates the adverse impacts of these attacks on the distribution system operations. Both attack types, in fact, affect the planning and operation aspects. In particular, the attack increases the PV capacity at bus 671, indicating a slight contribution from Type A attack to the adjustment of PV planning. Conversely, the capacity at buses 633 or 645 may decrease after the attack, attributable to the Type B attack. In other words, the Type B attack escalates the PV curtailment owing to the undesired reduction in the load in the EVCS. In such scenarios, PV curtailment, which is inevitable, must be adequately exploited. The aforementioned results provide valuable insights for the system operator on how to approach the planning problem in the event of an attack and prepare for possible curtailment scenarios.

5.3. Comparison with SO and RO methods

The performance of the proposed DRO method is compared with that of the SO and RO methods. The SO model is implemented using the sample average approximation technique (Birge and Louveaux, 2011) with 1000 samples. The basic formulation of the RO model is provided in Appendix. To fairly compare the performance of the RO, DRO, and SO methods, the same weights of the objective functions are set to the aforementioned three methods under the five scenarios.

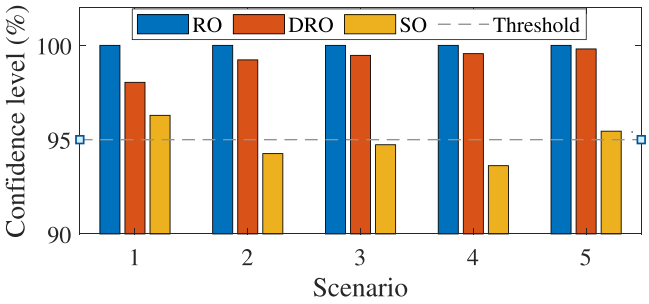

Fig. 8. Confidence levels of the RO, DRO, and SO methods in the IEEE 13-bus system.

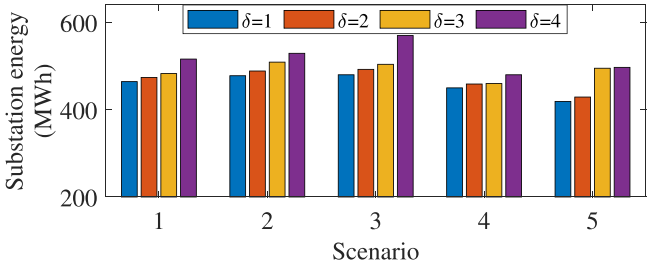

Fig. 9. Comparison of substation energies in five scenarios with varying Wasserstein radii δ in the IEEE 13-bus system.

Table 5 presents the average substation energies and total PV costs (i.e., the sum of PV deployment and curtailment costs) of the RO, DRO, and SO methods under the five scenarios. Note from this table that the RO and SO methods yield the highest and lowest substation energies and total PV costs, respectively. This phenomenon occurs because the RO satisfies all the constraints considering a worst-case scenario without any violation regardless of the probability distribution, whereas the actual data deviates from the actual distribution in the SO. The DRO outperforms these methods as it ensures a balance between the robustness of the solution and optimality with respect to the true distribution of the data. In terms of the sample efficiency, the DRO outperforms the SO with considerably fewer samples.

5.4. Out-of-sample test results

In the out-of-sample analysis, the confidence level can indicate the accuracy of all considered methods. The confidence level is defined as a criterion set by the chance-constrained model using the parameter β, such that each simulation scenario results in a solution without constraint violation with a probability of $(1-\beta)\times 100\%$. For this analysis, five scenarios containing different historical sample data are applied instead of using the predetermined distribution. In the case studies, the confidence level is set as 95%, which means that the probability of the violations under uncertainties should be lower than 5%. When the distribution of the scenario is accurate, the confidence level is guaranteed by both DRO and SO. However, the confidence level is not guaranteed by SO if the assumed probability distribution deviates from the real probability distribution. As shown in Fig. 8, the RO method maintains 100% robustness, the DRO method maintains a satisfactory level of approximately 98%, and the SO method fails in several scenarios.

5.5. Substation energy and total PV cost for different wasserstein radii δ

Fig. 9 shows the substation energy under five scenarios associated with different sets of samples with increasing δ. In general, the

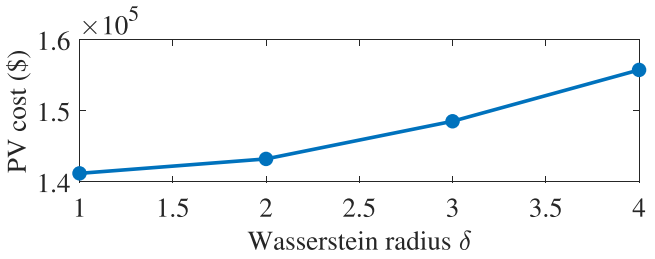

Fig. 10. Comparison of total PV costs with varying Wasserstein radii δ in the IEEE 13-bus system.

Table 6
Performance comparison for Cases 5 and 6 in the IEEE 13-bus system with either Type A or Type B attack.

Case	5		Type A attack		Type B attack	
Substation energy J_1 (MWh)	483.42		484.25		495.13	
Voltage imbalance J_2 (p.u)	61.17		60.83		63.26	
PV deployment cost J_3 (K$)	141		152		136	
PV curtailment cost J_4 ($)	204		162		245	
PV location	671	645	671	645	671	645
PV capacity (kVA)	225	96	231	101	210	67
PV curtailment (%)	0.4	3.8	0.5	1.8	1.1	8.9

substation energy increases with increasing δ. At large δ values, the substation energy is highly conservative because undesired distributions are included into the ambiguity set. Fig. 10 shows the total PV cost (PV installation and curtailment costs) with different parameter inputs of δ. The increasing Wasserstein radius affects the increment of the PV cost. This phenomenon occurs because a large δ is associated with a more conservative solution owing to the pathological distributions contained in the ambiguity set. Thereby, lower δ values are preferred to minimize the substation energy and total PV cost. However, a lower δ may not reflect various uncertain environments due to a less number of uncertainty samples in a smaller ambiguity set. On the aforementioned trade-off relationship, the DSOs may adaptively tune the Wasserstein radius to reduce the value of the objective function more or reflect the uncertainty further.

5.6. Occurrence of attack types

To further explore the attack types, the simulation of Case 5 is chosen as the baseline. The LAA is considered to occur at bus 645. Several charging poles are completely affected by either Type A or Type B attacks. The ratio of the attack is set to 20% of the available charging poles. Table 6 shows that attack affects mainly the size of the PV or the amount of curtailed PV power. When the bus suffers from a Type A attack, the PV deployment cost increases because the system must allocate higher load demand from the EVCS. However, the cost of curtailment decreases by 20.6% from $204 to $162. The Type B attack incurs a smaller PV size compared with that in Case 5 but increases the PV curtailment cost by 20.1% from $204 to $245. These results are attributable to the fact that the stochastic uncertainty is highly affected by the variability in the load demand, resulting from the charging demand in the EVCS. Type B attacks are characterized by a high substation energy and voltage imbalance because of less PV deployment and more PV curtailment. In conclusion, Type A attack affects the PV deployment, whereas Type B attack affects the PV curtailment. Therefore, the combination of both attack types is considered in this study to emphasize the previous baseline study.

5.7. Sensitivity analysis of the objective functions with respect to varying weights

The impact of varying weights on the objective functions $J_1 \sim J_4$ in the proposed DRO problem is quantified in Case 6–2. Fig. 11(a) compares the results between the substation energy (J_1) and voltage imbalance (J_2) with respect to varying ω_1 ($\omega_1 = 0.1, 1, 10, 25, 50$) given the fixed $\omega_2 = 0.5, \omega_3 = 1.2$, and $\omega_4 = 2$. We observe from this figure that there exists a trade-off relationship between the substation energy and voltage imbalance according to changes in ω_1. In other words, a higher (or lower) ω_1 yields a lower (or higher) substation energy; however, it yields a higher (or lower) voltage imbalance. Fig. 11(b) compares the results between the PV deployment cost (J_3) and PV curtailment cost (J_4) with respect to varying ω_3 ($\omega_3 = 0.1, 0.5, 1.2, 2, 3$) given the fixed $\omega_1 = 10, \omega_2 = 0.5$, and $\omega_4 = 2$. As expected, it is observed from this figure that the objective functions J_3 and J_4 have a trade-off relationship between the reduction of the PV deployment and curtailment costs in terms of the weight ω_3. Based on the aforementioned simulation results, DSOs may adaptively adjust these weights to situations in which they aim to perform their own purposes according to a trade-off relationship between the objective functions in terms of the weights.

Table 7
Performance comparison for Cases 5 and 6 in the IEEE 13-bus system with different EV charging rates.

Case	5		Type A attack		Type B attack	
Substation energy J_1 (MWh)	629.32		683.52		689.74	
Voltage imbalance J_2 (p.u)	65.72		67.37		68.05	
PV deployment cost J_3 (K$)	162		183		167	
PV curtailment cost J_4 ($)	204		162		245	
PV location	671	645	671	645	671	645
PV capacity (kVA)	240	102	243	120	253	94
PV curtailment (%)	0.6	2.8	0.7	0.8	1.2	7.1

Table 8
Performance of Case 4 in the IEEE 37-bus system.

Case	4-1 (bus 703)	4-2 (bus 706)	4-3 (bus 710)
Substation energy (MWh)	496.82	503.60	505.97
Voltage imbalance (p.u)	220.75	219.84	221.26

5.8. Validation of the proposed DRO model with different EV charging rates

The performance of the proposed DRO approach in Cases 5 and 6 is assessed in the IEEE 13-bus system with three EVCSs that have the charging poles with different charging rates. Each EVCS is assumed to have 68 charging poles with different maximum charging powers as follows: (i) 40 charging poles with 8 kW, (ii) 20 charging poles with 12 kW, (iii) 5 charging poles with 120 kW, and (iv) 3 charging poles with 240 kW. The total charging demand of each EVCS with different EV charging rates increases around 1240 kW. Note from Table 7 that, due to a significant increase of the EV charging demand, the substation energy, voltage imbalance, and PV deployment cost with different EV charging rates increase more than those with uniform EV charging rates shown in Table 6. Note also from Table 7 that Type A (or Type B) attack at bus 645 increases the PV deployment cost (or PV curtailment cost) due to their attack characteristics, which is consistent with the result in Table 6.

5.9. Scalability

Tables 8 and 9 present the results of Cases 4 and 6 in the IEEE 37-bus system, respectively. Compared with those in Case 4, the substation energies and voltage imbalances in Case 6 for the attack on bus {703, 706, 710} are reduced by {25%, 26.6%, 24.6%} and {15.2%, 18.3%, 17.8%}, respectively, indicating the effectiveness of the proposed approach. Table 9 shows that the performance of the DRO method depends on the attack location, which affects the added PV capacity, curtailment, and cost. Type A attacks affect the added PV capacities, and PV curtailments can be implemented to address Type B attacks. In cases involving insufficient PV capacity, new PV systems

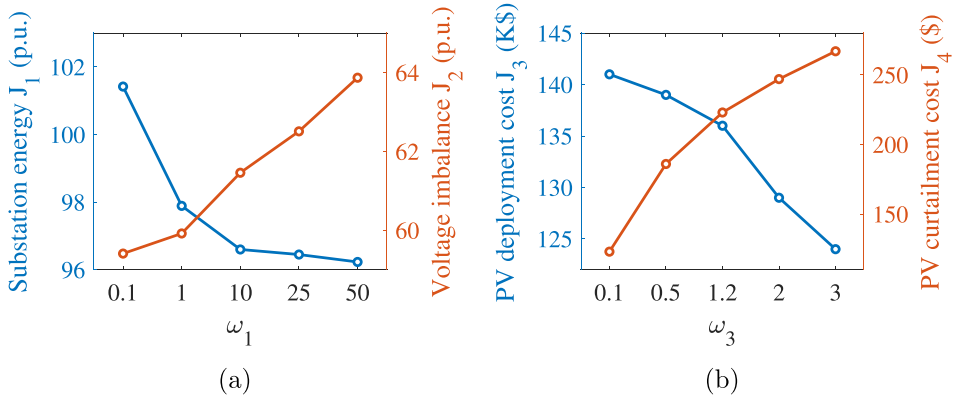

Fig. 11. Sensitivity analysis of the objective functions with respect to varying weights: (a) ω_1 ($\omega_2 = 0.5, \omega_3 = 1.2, \omega_4 = 2$) and (b) ω_3 ($\omega_1 = 10, \omega_2 = 0.5, \omega_4 = 2$).

Table 9
Performance of Case 6 in the IEEE 37-bus system.

Case	6-1 (bus 703)	6-2 (bus 706)	6-3 (bus 710)
Substation energy J_1 (MWh)	372.6	369.57	381.18
Voltage imbalance J_2 (p.u)	187.13	179.59	181.95
PV deployment cost J_3 (K$)	44	47	40
PV curtailment cost J_4 ($)	301	275	289
PV location	711 725 744	725 744	711 744
PV capacity (kVA)	14 4 26	32 15	23 17
PV curtailment (%)	0.4 1.3 0.8	1.3 1.9	2.2 3.6

Table 10
Computation time (s) of the proposed DRL method in IEEE 13-bus and 37-bus systems.

Test System	Case 5	Case 6–1	Case 6-2
IEEE 13-bus system	192	216	218
IEEE 37-bus system	1052	1193	1258

are not necessarily installed. Instead, the capacities of the existing PV systems are supplemented. The PV capacities are not added in each case, and the addition depends on the attack scenario. These results demonstrate the applicability of the proposed approach in the IEEE 37-bus system. Table 10 shows the computation time of the proposed DRO method for Cases 5, 6–1, and 6–2 in the IEEE 13-bus and 37-bus systems. Note from this table that the computation time with attack (Cases 6–1 and 6–2) is larger than that without attack (Case 5) in both systems. In addition, as expected, it is observed that the computation time in the IEEE 37-bus system is larger than that in the IEEE 13-bus system. From the perspective of the planning problem of PV systems, these results demonstrate that the proposed DRO approach is computationally efficient and applicable for the deployment and curtailment of PV systems that mitigate LAA against EVCS in the presence of PV/load uncertainties.

5.10. Verification of the linear power flow model in the IEEE 13-bus and 37-bus systems

The performance between the linear and nonlinear power flow models in the proposed approach is compared in terms of voltage magnitude and substation energy. The nonlinear power flow is calculated by the Newton-iterative method using OpenDSS. Fig. 12 compares the voltage magnitude and substation energy between the linear and nonlinear power flow models in the IEEE 13-bus system, respectively. Note from these figures that the maximum (average) error of voltage magnitude/substation energy is computed as 0.0031 p.u./0.0212 p.u. (0.0022 p.u./0.0048 p.u.). Fig. 13 compares the voltage magnitude and substation energy between the linear and nonlinear power flow models in the IEEE 37-bus system, respectively. Note from these figures that the maximum (average) error of voltage magnitude/substation energy is computed as 0.0029 p.u./0.0189 p.u. (0.0021 p.u./0.0074 p.u.). Based on the aforementioned results with a small error between the linear and nonlinear power flow models, the linear power flow model adopted to this study is quite accurate.

The novelty and valuable observations of the proposed method are summarized as follows.

- To the best of authors' knowledge, the proposed approach is the first PV planning/curtailment-integrated DRO-based VVO framework that maintains reliable and robust three-phase unbalanced distribution system operations while addressing the uncertainties of both PV generation output/load and LAA against EVCS.
- *Improvement of solution feasibility:* The proposed DRO method resolves the solution infeasibility issue that occurs in the DO method under the LAA in the presence of uncertain PV generation output and load (compare the results of Sections 5.2.1 and 5.2.2).
- *LAA impact mitigation via PV planning and curtailment:* The DRO with the planning/curtailment stage (Cases 5 and 6) reduces the substation energy and voltage imbalance more significantly than the DRO without the planning/curtailment stage (Cases 3 and 4) (compare the results of Tables 3 and 4).
- *Robust location and capacity upgrade of PV systems against LAA:* To mitigate the impact of the LAA on distribution grid operation, in general the location of new PV systems and capacity upgrade of existing PV systems are determined according to the following two factors: (i) the location of attacked EVCSs and (ii) the location of PV systems adjacent to the attacked EVCSs (see the results of Tables 4 and 9).
- *Impact analysis of PV planning/curtailment subject to two types of LAAs:* Type A attack increases the PV deployment cost and Type B attack increases the PV curtailment cost. This is because the former and latter attacks increase and decrease the EV charging demands, respectively (see the results of Tables 6 and 7).
- *Sample efficiency:* Compared to the RO and SO method with 1000 samples, the proposed DRO method with 20 samples yields a less conservative solution and sample efficiency along with the satisfaction of confidence level (see the results of Table 5 and Fig. 8).

6. Conclusions

This paper proposes a DRO-based VVO framework that mitigates the impact of LAAs on EVCSs while addressing the uncertainties of PV generation output and load in a three-phase unbalanced distribution system. The key parts of the proposed framework include the following two tasks: (i) a formulation of the DRO-based VVO problem using a Wasserstein metric-based ambiguity set to handle the uncertainties of PV generation output and load and (ii) an integration of PV planning and curtailment process into the DRO-based VVO problem to mitigate

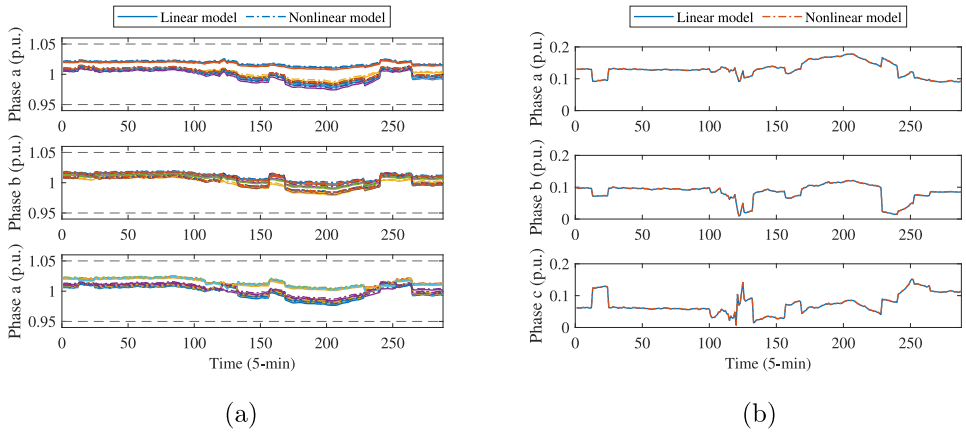

Fig. 12. Performance comparison of the linear and nonlinear power flow models in the IEEE 13-bus system: (a) voltage magnitude and (b) substation energy.

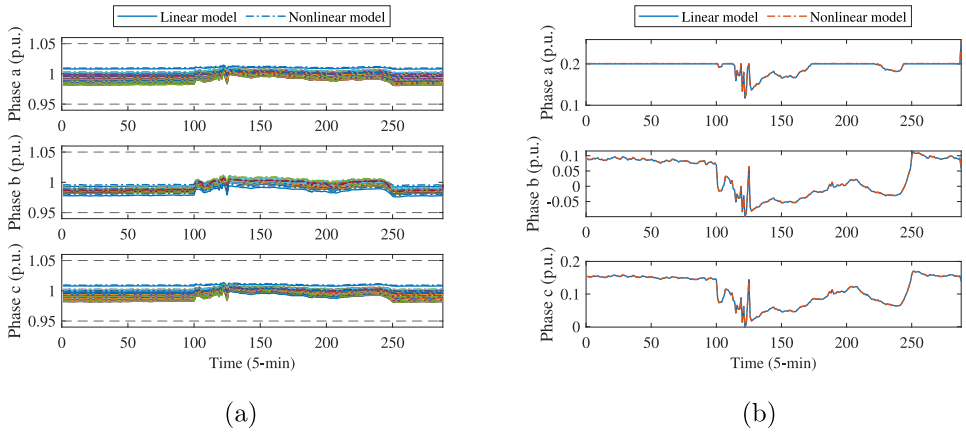

Fig. 13. Performance comparison of the linear and nonlinear power flow models in the IEEE 37-bus system: (a) voltage magnitude and (b) substation energy.

the detrimental impact of LAAs on EVCS. Furthermore, to use off-the-shelf optimization solvers, the chance constraints of voltage, current, and curtailed PV power in the DRO problem are reformulated into tractable deterministic constraints based on the strong duality theory. Numerical examples over IEEE 13-bus and 37-bus systems demonstrate the effectiveness of the proposed framework in successfully alleviating the substation energy and voltage imbalance by determining the optimal locations and capacity of PV systems along with its optimal real power curtailment under uncertain PV generation outputs/loads and LAAs on EVCSs. Furthermore, the proposed DRO method outperforms the state-of-the-art SO and RO methods in terms of the out-of-sample confidence levels.

In future work, there are two research work efforts extended from the proposed approach: (i) to build a realistic DRO-based VVO framework where legacy voltage regulating devices (e.g., on-load tap changers and capacitor banks) and inverters of PV systems cooperate to address the natural and artificial uncertainties and (ii) to develop a planning algorithm that determines optimal locations of smart EVCSs integrated with the PV system and energy storage system, which are robust to LAAs on EVCSs.

CRediT authorship contribution statement

Panggah Prabawa: Conceptualization, Investigation, Methodology, Writing – original draft. **Dae-Hyun Choi:** Supervision, Writing – review & editing.

Declaration of competing interest

The authors declare that they have no known competing financial interests or personal relationships that could have appeared to influence the work reported in this paper.

Data availability

No data was used for the research described in the article.

Acknowledgments

This work was supported in part by Basic Science Research Program through the National Research Foundation of Korea (NRF), Republic of Korea funded by the Ministry of Education under Grant 2022R1F1A1062888, and in part by the NRF, Republic of Korea grant funded by the Korea government (MSIT) under Grant RS-2023-00255695.

Appendix. Formulation of RO model

For the simulation of the RO method, the constraints of the voltage magnitude (20), current magnitude (21), and curtailed PV real

power (29) limits are replaced by their corresponding robust counterparts using the results in Li et al. (2011). Consider the following general optimization problem

$$\min \sum_j \mathcal{J}(x_j)$$

s.t.

$$\sum_j \widetilde{a}_{ij} x_j \le \widetilde{b}_i, \quad \forall i$$

where x_j is the jth decision variable, and $\widetilde{a}_{ij}$ and $\widetilde{b}_i$ represent the actual values of the parameters subject to uncertainty in the jth decision variable associated with the ith constraint. The uncertainty-induced $\widetilde{a}_{ij}$ and $\widetilde{b}_i$ are expressed as

$$\widetilde{a}_{ij} = a_{ij} + \xi_{ij}\widehat{a}_{ij}$$
$$\widetilde{b}_i = b_i + \xi_i \widehat{b}_i$$

where a_{ij} and b_i represent the nominal values of the parameters; $\widehat{a}_{ij}$ and $\widehat{b}_i$ represent constant perturbation; and ξ_{ij} and ξ_i are random variables that are subject to uncertainty. Using the expressions of $\widetilde{a}_{ij}$ and $\widetilde{b}_i$ along with a predefined uncertainty set $\mathcal{U}$, the original constraint is reformulated as follows:

$$\sum_j a_{ij} x_j + \left[\max_{\xi \in \mathcal{U}} \left\{ \sum_j \xi_{ij} \widehat{a}_{ij} x_j - \xi_i \widehat{b}_i \right\}\right] \le b_i.$$

Based on the duality theory and the box uncertainty set $\mathcal{U}_\infty = \{\xi || \xi_j | \le \Gamma_i, \forall j\}$, the final robust counterpart is written as

$$\sum_j a_{ij} x_j + \Gamma_i \left[\sum_j \widehat{a}_{ij} |x_j| + \widehat{b}_i \right] \le b_i$$

where $\Gamma_i \ge 0$ is a parameter that controls the level of robustness.

References

Acharya, S., Dvorkin, Y., Karri, R., 2020a. Public plug-in electric vehicles + grid data: Is a new cyberattack vector viable? IEEE Trans. Smart Grid 11 (6), 5099–5113. http://dx.doi.org/10.1109/tsg.2020.2994177.

Acharya, S., Dvorkin, Y., Pandžić, H., Karri, R., 2020b. Cybersecurity of smart electric vehicle charging: A power grid perspective. IEEE Access 8, 214434–214453. http://dx.doi.org/10.1109/access.2020.3041074.

Al Abri, R., El-Saadany, E.F., Atwa, Y.M., 2013. Optimal placement and sizing method to improve the voltage stability margin in a distribution system using distributed generation. IEEE Trans. Power Syst. 28 (1), 326–334. http://dx.doi.org/10.1109/tpwrs.2012.2200049.

Ali, A., Mahmoud, K., Raisz, D., Lehtonen, M., 2021. Probabilistic approach for hosting high PV penetration in distribution systems via optimal oversized inverter with watt-VAr functions. IEEE Syst. J. 15 (1), 684–693. http://dx.doi.org/10.1109/jsyst.2020.2982467.

Andrianesis, P., Caramanis, M., Li, N., 2022. Optimal distributed energy resource coordination: A decomposition method based on distribution locational marginal costs. IEEE Trans. Smart Grid 13 (2), 1200–1212. http://dx.doi.org/10.1109/tsg.2021.3123284.

Basnet, M., Ali, M.H., 2023. Deep reinforcement learning-driven mitigation of adverse effects of cyber-attacks on electric vehicle charging station. Energies 16 (21), 7296. http://dx.doi.org/10.3390/en16217296.

Bazrafshan, M., Gatsis, N., 2018. Comprehensive modeling of three-phase distribution systems via the bus admittance matrix. IEEE Trans. Power Syst. 33 (2), 2015–2029. http://dx.doi.org/10.1109/tpwrs.2017.2728618.

Bernstein, A., Dall'Anese, E., 2017. Linear power-flow models in multiphase distribution networks. In: 2017 IEEE PES Innovative Smart Grid Technologies Conference Europe. ISGT-Europe, IEEE, pp. 1–6. http://dx.doi.org/10.1109/isgteurope.2017.8260205.

Bernstein, A., Wang, C., Dal'Anese, E., Le Boudec, J.-Y., Zhao, C., 2018. Load flow in multiphase distribution networks: Existence, uniqueness, non-singularity and linear models. IEEE Trans. Power Syst. 33 (6), 5832–5843. http://dx.doi.org/10.1109/tpwrs.2018.2823277.

Birge, J.R., Louveaux, F., 2011. Introduction To Stochastic Programming, second ed. Springer Science & Business Media, http://dx.doi.org/10.1007/978-1-4614-0237-4.

Budiman, F.N., Ramli, M.A., Milyani, A.H., Bouchekara, H.R., Rawa, M., Muktiadji, R.F., Seedahmed, M.M., 2022. Stochastic optimization for the scheduling of a grid-connected microgrid with a hybrid energy storage system considering multiple uncertainties. Energy Rep. 8, 7444–7456. http://dx.doi.org/10.1016/j.egyr.2022.05.249.

Cai, C., Chen, J., Xi, M., Tao, Y., Deng, Z., 2020. Multi-objective planning of distributed photovoltaic power generation based on multi-attribute decision making theory. IEEE Access 8, 223021–223029. http://dx.doi.org/10.1109/access.2020.3042010.

Cheng, Z., Yue, D., Shen, S., Hu, S., Chen, L., 2022. Secure frequency control of hybrid power system under DoS attacks via lie algebra. IEEE Trans. Inf. Forensics Secur. 17, 1172–1184. http://dx.doi.org/10.1109/tifs.2022.3158550.

ElHussini, H., Assi, C., Moussa, B., Atallah, R., Ghrayeb, A., 2021. A tale of two entities: Contextualizing the security of electric vehicle charging stations on the power grid. ACM Trans. Internet Things 2 (2), 1–21. http://dx.doi.org/10.1145/3437258.

Gao, R., Kleywegt, A., 2023. Distributionally robust stochastic optimization with wasserstein distance. Math. Oper. Res. 48 (2), 603–655. http://dx.doi.org/10.1287/moor.2022.1275.

Guo, Y., Baker, K., Dall'Anese, E., Hu, Z., Summers, T.H., 2019. Data-based distributionally robust stochastic optimal power flow— part I: Methodologies. IEEE Trans. Power Syst. 34 (2), 1483–1492. http://dx.doi.org/10.1109/tpwrs.2018.2878385.

Guo, Z., Wei, W., Chen, L., Wang, Z., Catalão, J.P., Mei, S., 2022. Optimal energy management of a residential prosumer: A robust data-driven dynamic programming approach. IEEE Syst. J. 16 (1), 1548–1557. http://dx.doi.org/10.1109/jsyst.2020.3043342.

IEEE-PES, 2015. Open data sets. URL https://site.ieee.org/pes-iss/data-sets/. (Accessed on 29 August 2022).

Jabr, R.A., 2013. Adjustable robust OPF with renewable energy sources. IEEE Trans. Power Syst. 28 (4), 4742–4751. http://dx.doi.org/10.1109/tpwrs.2013.2275013.

Kim, D., Kim, H., Won, D., 2020. Operation strategy of shared ESS based on power sensitivity analysis to minimize PV curtailment and maximize profit. IEEE Access 8, 197097–197110. http://dx.doi.org/10.1109/access.2020.3034339.

Kou, P., Liang, D., Gao, L., 2018. Stochastic energy scheduling in microgrids considering the uncertainties in both supply and demand. IEEE Syst. J. 12 (3), 2589–2600. http://dx.doi.org/10.1109/jsyst.2016.2614723.

Li, Z., Ding, R., Floudas, C.A., 2011. A comparative theoretical and computational study on robust counterpart optimization: I. Robust linear optimization and robust mixed integer linear optimization. Ind. Eng. Chem. Res. 50 (18), 10567–10603. http://dx.doi.org/10.1021/ie200150p.

Liang, G., Weller, S.R., Zhao, J., Luo, F., Dong, Z.Y., 2017. The 2015 Ukraine blackout: Implications for false data injection attacks. IEEE Trans. Power Syst. 32 (4), 3317–3318. http://dx.doi.org/10.1109/tpwrs.2016.2631891.

Liang, G., Weller, S.R., Zhao, J., Luo, F., Dong, Z.Y., 2019. A framework for cyber-topology attacks: Line-switching and new attack scenarios. IEEE Trans. Smart Grid 10 (2), 1704–1712. http://dx.doi.org/10.1109/tsg.2017.2776325.

Liu, M.Z., Procopiou, A.T., Petrou, K., Ochoa, L.F., Langstaff, T., Harding, J., Theunissen, J., 2020. On the fairness of PV curtailment schemes in residential distribution networks. IEEE Trans. Smart Grid 11 (5), 4502–4512. http://dx.doi.org/10.1109/tsg.2020.2983771.

Liu, Z., Wang, L., 2022. A robust strategy for leveraging soft open points to mitigate load altering attacks. IEEE Trans. Smart Grid 13 (2), 1555–1569. http://dx.doi.org/10.1109/tsg.2021.3134176.

Mohsenian-Rad, A.-H., Leon-Garcia, A., 2011. Distributed internet-based load altering attacks against smart power grids. IEEE Trans. Smart Grid 2 (4), 667–674. http://dx.doi.org/10.1109/tsg.2011.2160297.

Nasiri, N., Zeynali, S., Ravadanegh, S.N., 2023. Tactical participation of a multienergy system in distributionally robust wholesale electricity market under high penetration of electric vehicles. IEEE Syst. J. 17 (1), 1465–1476. http://dx.doi.org/10.1109/jsyst.2022.3221490.

Nguyen, H.T., Choi, D.-H., 2023. Decentralized distributionally robust coordination between distribution system and charging station operators in unbalanced distribution systems. IEEE Trans. Smart Grid 14 (3), 2164–2177. http://dx.doi.org/10.1109/tsg.2022.3210232.

Schermeyer, H., Vergara, C., Fichtner, W., 2018. Renewable energy curtailment: A case study on today's and tomorrow's congestion management. Energy Policy 112, 427–436. http://dx.doi.org/10.1016/j.enpol.2017.10.037.

Singh, S., Pamshetti, V.B., Thakur, A.K., Singh, S.P., 2020. Multistage multiobjective volt/VAR control for smart grid-enabled cvr with solar PV penetration. IEEE Syst. J. 15 (2), 2767–2778. http://dx.doi.org/10.1109/jsyst.2020.2992985.

Sun, B., Li, Y., Zeng, Y., Chen, J., Shi, J., 2022. Optimization planning method of distributed generation based on steady-state security region of distribution network. Energy Rep. 8, 4209–4222. http://dx.doi.org/10.1016/j.egyr.2022.03.078.

Tran, N.N., Pota, H.R., Tran, Q.N., Hu, J., 2021. Designing constraint-based false data-injection attacks against the unbalanced distribution smart grids. IEEE Internet Things J. 8 (11), 9422–9435. http://dx.doi.org/10.1109/jiot.2021.3056649.

Wang, C., Liu, C., Chen, J., Zhang, G., 2024. Cooperative planning of renewable energy generation and multi-timescale flexible resources in active distribution networks. Appl. Energy 356, 122429. http://dx.doi.org/10.1016/j.apenergy.2023.122429.

Wu, Q., Nielsen, A.H., Østergaard, J., Cha, S.T., Marra, F., Chen, Y., Træholt, C., 2010. Driving pattern analysis for electric vehicle (EV) grid integration study. In: 2010 IEEE PES Innovative Smart Grid Technologies Conference Europe. ISGT-Europe, IEEE, pp. 1–6. http://dx.doi.org/10.1109/isgt.2010.5743083.

Wu, X., Qi, S., Wang, Z., Duan, C., Wang, X., Li, F., 2019. Optimal scheduling for microgrids with hydrogen fueling stations considering uncertainty using data-driven approach. Appl. Energy 253, 113568. http://dx.doi.org/10.1016/j.apenergy.2019.113568.

Xie, W., 2019. On distributionally robust chance constrained programs with wasserstein distance. Math. Program. 186 (1–2), 115–155. http://dx.doi.org/10.1007/s10107-019-01445-5.

Zhang, Q., Bu, F., Guo, Y., Wang, Z., 2024. Tractable data enriched distributionally robust chance-constrained conservation voltage reduction. IEEE Trans. Power Syst. 39, 821–835. http://dx.doi.org/10.1109/tpwrs.2023.3244895.

Zhang, H., Moura, S.J., Hu, Z., Qi, W., Song, Y., 2018a. Joint PEV charging network and distributed PV generation planning based on accelerated generalized benders decomposition. IEEE Trans. Transp. Electrif. 4 (3), 789–803. http://dx.doi.org/10.1109/tte.2018.2847244.

Zhang, C., Xu, Y., Dong, Z.Y., 2018b. Probability-weighted robust optimization for distributed generation planning in microgrids. IEEE Trans. Power Syst. 33 (6), 7042–7051. http://dx.doi.org/10.1109/tpwrs.2018.2849384.